MDPI

Article

Active Disturbance Rejection Control for Robust Flight of a Passively Tilted Hexarotor

Santos M. Orozco-Soto [1]*, Jonathan Cacace [1,2], Fabio Ruggiero [1,2] and Vincenzo Lippiello [1,2]

[1] Consorzio C.R.E.A.T.E., Via Claudio 21, Naples, 80125, Italy.
[2] Department of Electrical Engineering and Information Technology, University of Naples Federico II, Via Claudio 21, Naples, 80125, Italy.
* Correspondence: sorozco@ctrl.cinvestav.mx

Abstract: This paper presents a robust control strategy for controlling the flight of a passively (fixed) tilted hexarotor unmanned aerial vehicle (UAV). The proposed controller is based on a robust extended-state observer to estimate and reject internal dynamics and external disturbances at run-time. Both stability and convergence of the observer are proved using Lyapunov-based perturbation theory and an ultimate bound approach. Such a controller is implemented within a highly realistic simulation environment that includes physics motors, devising an almost transparent behaviour with respect to the real UAV. The controller is tested for flying under normal conditions and in the presence of different types of disturbances showing successful results. Furthermore, the proposed control system is compared against another robust control approach, presenting a better performance regarding the attenuation of the error signals.

Keywords: Passively tilted hexarotor; Robust UAV control; Active disturbance rejection Control; Sliding-mode extended-state observer

1. Introduction

The increasing use of multirotor unmanned aerial vehicles (UAV) in a broad set of applications demands, in some cases, the use of 6-degree-of-freedom (DOF) motions. In other words, simultaneous translational and rotational motions are required. For the case of quadrotors, 6-DOF actuation is not possible since they have only four actuators placed in a flat (co-planar) configuration. Increasing the number of rotors in such a flat configuration does not change the situation, even though they can cope with some actuation faults. Adding a tilting angle to the rotors produces forces so that the drone becomes a fully actuated device within the 6-DOF Cartesian space. Such a tilting angle can be either fixed (passive) or actuated by an auxiliary motor (active).

Besides external disturbances, such as vortexes, wind gusts, or payload that might affect a UAV, another significant drawback often present when controlling real devices is the uncertainty about the parameters of the system's dynamic model. Thus, a control problem for passively tilted hexarotors is to fly to the target pose or trajectory with respect to the world reference frame and to remain steadily within some desired tolerances about them despite the external disturbances and inaccuracy of the dynamic model. In this context, control researchers and engineers have developed robust techniques to deal with dynamic systems' disturbances and uncertainties, and the UAVs' case is not an exception.

Several robust controllers for both tilted and non-tilted hexarotors can be found in the literature. In addition to PID-type controllers for non-tilted hexacopters [1,2], another common control technique for flat hexarotors is the Active Disturbance Rejection Control (ADRC)-type approach. The advantage of using these last controllers is that they can deal with external disturbances and do not depend on an accurate dynamic model. There are plenty of recently-reported successful regulation and tracking simulations using this control approach –or its variations–, which is applied to both non-tilted and actively tilted

Citation: Orozco-Soto, S. M.; Cacace, J.; Ruggiero F.; Lippiello, V. Active Disturbance Rejection Control for Robust Flight of a Passively Tilted Hexarotor. *Drones* **2022**, *1*, 0. https://doi.org/

Received:
Accepted:
Published:

hexarotors [3–7]; nevertheless, the closed-loop stability is only proved in [3,4] and the observer's convergence proof is only present in [3]. It is worth remarking that in [3,4], the ADRC stability proof relies on the *a priori* assumption that the total disturbance is bounded, which is not applicable to fully actuated multirotor UAVs as is later explained in the text.

On the other hand, extensive literature with successful simulations is also available for robust control of passively tilted hexarotors. Robust integral of the sign of the error (RISE) [8], integral sliding mode control (SMC) [9], adaptive SMC [10], and super twisting observer SMC [11] techniques are also reported. It is worth mentioning that these control schemes are enhanced versions of the SMC to reduce its intrinsic *chattering* effect. Furthermore, an adaptive control scheme was also presented in simulation [12]. Although this last technique is robust upon parametric uncertainties, it is still susceptible to external disturbances. To the best of the authors' knowledge, the only robust controllers reported in the literature that were implemented in actual passively tilted hexacopters are port-Hamiltonian-based approaches [13,14]; these passivity-based techniques suffer from time-varying parametric uncertainties and non-smooth disturbances.

In the context of disturbance compensation of multirotor UAVs, the following problems have been found so far. i) The use of a tilting angle for the rotors helps to produce 6 DOF Cartesian motion; however, a significant drawback of actively tilting the rotors, despite the hardware implications, is that the actuator dynamics delay the instantaneous disturbance rejection [15]. ii) ADRC-type techniques are robust external disturbances estimation and compensation tools. Their main drawback is that the theory assumes that there exist bounds for the total disturbances, which are compound by external wrenches and internal terms of the plant that are different from a *cascade of integrators* representation [16]. Such an assumption does not hold for the case of fully actuated multirotors, since state-dependent disturbances present in the model cannot be assumed bounded.

This work addresses the robust flight problem of a passively tilted hexarotor. In order to deal with external disturbance and uncertainty, a robust control approach is implemented. Such a proposal falls within the ADRC category since it rejects the disturbances by estimating and compensating for them using a proposed sliding-mode extended-state observer (SMESO). In addition, the observer's stability and convergence are proved using Lyapunov-based perturbation theory and an ultimate bound approach. The developed controller is implemented on a custom hexarotor model[1], adequately adapted to have tilted rotors and that runs within Gazebo[2], a 3D simulator with physics motors which is almost transparent with respect to the real version of such a UAV. Both the controller and the robust ESO are executed as nodes of the Robotics Operating System (ROS) middleware[3], which allows the simultaneous execution of such algorithms. The experiments to test the developed controller consisted of i) performing a given trajectory; ii) feeding target poses to the UAV such that it flights under wind conditions and payload provided by the simulator; and iii) carrying out a comparison against an SMC for pose regulation. The contributions of this work are listed below.

- The application of the ADRC to a passively tilted hexarotor has not been reported up to the best authors' knowledge. The closest related works use actively tilted or fixed hexarotors, which are disadvantaged in actuation and disturbance rejection capabilities with respect to passively tilted hexarotors. Furthermore, our version of the ADRC technique is enhanced with a sliding-mode observer, whose advantages are mentioned later in the text.
- Both the controller and observer stability analyses are presented. The implementation of a SMESO based ADRC algorithm in a passively tilted hexarotor is novel in the literature up to the best authors' knowledge; furthermore, the stability proof of the

[1] This model is available at the following repository: https://github.com/jocacace/Firmware.
[2] http://gazebosim.org
[3] http://www.ros.org

presented ADRC does not depend on *a priori* assumptions of the boundaries of the total disturbance as the traditional ADRC scheme requests, but only in its differentiation properties.

- Our controller is implemented in a highly realistic simulation environment, completely different from a traditional numerical simulation. This is a step towards the successful implementation on a real device since our simulation scheme is almost transparent with the real version of the platform. Additionally, our results are shown in a video.
- The comparison against another robust control and observation strategy favours the controller developed in this work. The proposed design is indeed a competitive alternative to control passively tilted hexarotors UAVs, and it is not limited to the presented specific problem. The proposed controller applies to other passively-tilted multirotors by selecting the appropriate allocation matrix, tuning both the controller and observer gains, and adjusting the integration steps.

The rest of the paper is organised as follows. Section 2 addresses the theory of ADRC, sliding mode observers and finding bounds for state-dependent disturbances; the dynamics of the hexarotor UAV is presented as well in that section. Section 3 details the controller design and stability. Section 4 describes how the controller is implemented. The case studies are presented in 5 and finally, Section 6 concludes the paper.

2. Theoretical Background

ADRC is a control technique in which success relies on estimating and rejecting an unknown total disturbance using an ESO. In this case, a nonlinear control problem is reduced to a *cascade of integrators* one. Therefore, this control technique can deal with a vast range of uncertainties and disturbances [16]. Below, an overview of the mentioned control approach and a robust observation scheme can be found. As stated before, ADRC's theory rely on *a priori* assumptions of the existence of boundaries for the disturbances affecting the controlled system. For the case of external disturbances, such assumptions are reasonable; however, state-dependent disturbances cannot be assumed bounded. Hence, some useful theorems retrieved from the literature that are beneficial for the derivation of the stability proofs are also addressed in this section.

2.1. Active Disturbance Rejection Control

Consider the following multiple-input multiple-output (MIMO) uncertain nonlinear system subjected to external disturbances [17], which is expressed in a *chain of integrators* canonical form[4]

$$\begin{cases} \dot{x}_{i,1}(t) = x_{i,2}(t) \\ \dot{x}_{i,2}(t) = x_{i,3}(t) \\ \quad \vdots \\ \dot{x}_{i,n_i}(t) = \varsigma_i(\mathbf{x}(t)) + \boldsymbol{\xi}_i(\mathbf{x}(t))\mathbf{u}(t) + \boldsymbol{\zeta}_i(t) \\ y_i(t) = h_i(\mathbf{x}(t)) \end{cases} \tag{1}$$

with $i = 1, \ldots, m$, and where $x_{i,j}(t) \in \mathbb{R}$ is a component of the vector state $\mathbf{x}(t) = \begin{bmatrix} x_{1,1}(t) & \cdots & x_{1,n_1}(t) & \cdots & x_{m,1}(t) & \cdots & x_{m,n_m}(t) \end{bmatrix}^T \in \mathbb{R}^{(n_1+\cdots+n_m)}$, with $j = 1, \ldots, n_i$ and $n_i > 0$; $y_i(t) \in \mathbb{R}$ is the $i-$th output component; $\mathbf{u}(t) = \begin{bmatrix} u_1(t) & \cdots & u_m(t) \end{bmatrix} \in \mathbb{R}^m$ is the control inputs vector; $\boldsymbol{\varsigma}(\mathbf{x}(t)) = \begin{bmatrix} \varsigma_1(\mathbf{x}(t)) & \cdots & \varsigma_m(\mathbf{x}(t)) \end{bmatrix}^T \in \mathbb{R}^m$ is the dynamics function with uncertain parameters; $\boldsymbol{\xi}_i(\mathbf{x}(t)) \in \mathbb{R}^{1\times m}$ is the row of a non singular uncertain matrix $\boldsymbol{\Xi} \in \mathbb{R}^{m\times m}$ depending on the system's state; $h_i(\mathbf{x}(t)) \in \mathbb{R}$ is a function of the states; and $\boldsymbol{\zeta}(t) = \begin{bmatrix} \zeta_1(t) & \cdots & \zeta_m(t) \end{bmatrix}^T \in \mathbb{R}^m$ is the external disturbances vector, usually unknown but bounded. In order to reduce (1) to a chain of integrators regulation problem,

[4] If the system is not represented as a *chain of integrators* canonical form, the corresponding transformations must be performed to lead the system to such a form.

the whole uncertain dynamics and the external disturbances can be embedded into the following *total disturbance* [16]

$$\varsigma(\mathbf{x}(t)) + \mathbf{\Delta}_{\Xi}(\mathbf{x}(t))\mathbf{u}(t) + \boldsymbol{\zeta}(t) \triangleq \mathbf{x}(t)_{n+1}, \tag{2}$$

where $\mathbf{\Delta}_{\Xi}(\mathbf{x}(t)) = \mathbf{\Xi}(\mathbf{x}(t)) - \widetilde{\mathbf{\Xi}}(\mathbf{x}(t)) \in \mathbb{R}^{m\times m}$ is an approximation[5] of $\mathbf{\Xi}(\mathbf{x}(t))$. The vector $\mathbf{x}(t)_{n+1} = \left[x_{1,n_1+1} \cdots x_{m,n_m+1}\right] \in \mathbb{R}^m$ is a virtual augmented state whose estimate $\hat{\mathbf{x}}(t)_{n+1} \in \mathbb{R}^m$ contain all the *total disturbances* and it can be retrieved through the following ESO [17]

$$\begin{cases} \dot{\hat{x}}_{i,1} = \hat{x}_{i,2} + \varepsilon^{n_i-1}\phi_{i,1}\left(\dfrac{x_{i,1}-\hat{x}_{i,1}}{\varepsilon^{n_i}}\right) \\ \dot{\hat{x}}_{i,2} = \hat{x}_{i,3} + \varepsilon^{n_i-2}\phi_{i,2}\left(\dfrac{x_{i,1}-\hat{x}_{i,1}}{\varepsilon^{n_i}}\right) \\ \quad \vdots \\ \dot{\hat{x}}_{i,n_i} = \hat{x}_{i,n_i+1} + \phi_{i,n_i}\left(\dfrac{x_{i,1}-\hat{x}_{i,1}}{\varepsilon^{n_i}}\right) + \widetilde{\mathbf{\Xi}}(\mathbf{x}(t))\mathbf{u}(t) \\ \dot{\hat{x}}_{i,n_i+1} = \dfrac{1}{\varepsilon}\Phi_{i,n_i+1}\left(\dfrac{x_{i,1}-\hat{x}_{i,1}}{\varepsilon^{n_i}}\right) \end{cases} \tag{3}$$

where $\hat{x}_{i,j}(t) \in \mathbb{R}$ is a component of the vector state estimate

$$\hat{\mathbf{x}}(t) = \begin{bmatrix} \hat{x}_{1,1}(t) & \cdots & \hat{x}_{1,n_1}(t) & \cdots & \hat{x}_{m,1}(t) & \cdots & \hat{x}_{m,n_m+1}(t) \end{bmatrix}^T \in \mathbb{R}^{(n_1+\cdots+(n_m+1))},$$

with $j = 1,\ldots,n_i$ and $i = 1,\ldots,m$; $\varepsilon > 0$ is a tuning constant, and $\phi_{i,j}(\cdot) \in \mathbb{R}$, with $j = 1,\ldots,n_i+1$, is a function that guarantees $x_{i,1} - \hat{x}_{i,1} \to 0$ as $t \to t_0$, with $0 < t_0 < \infty$ is a determined finite time. Notice that the dynamics of (3) must be significantly quicker than (1). Once the total disturbance is estimated, it can be used as feedback in the following controller for the system (1)

$$\mathbf{u}(t) = \widetilde{\mathbf{\Xi}}(\mathbf{x}(t))^{-1}\mathbf{u}_0(\mathbf{x}(t)) - \hat{\mathbf{x}}(t)_{n+1}, \tag{4}$$

where $\mathbf{u}_0(\mathbf{x}(t)) \in \mathbb{R}^m$ can be any linear control technique that regulates $\dot{\mathbf{x}}(t)$. Since (4) cancels out both internal uncertainties and external disturbances, it leads to the following control problem

$$\dot{\mathbf{x}}(t) \simeq \mathbf{u}_0(\mathbf{x}(t)). \tag{5}$$

2.2. Sliding Mode Observers

As it was mentioned before, the success of the controller (4) relies on the accurate estimation of the total disturbance (2) via the ESO. Hence, the key functionality of the ADRC is the observer. A common technique to develop an ESO is using a Luenberger observer. However, to enhance the ESO performance, some robust techniques like generalized proportional integral (GPI) observer and high gain observers were implemented in the literature [18,19]. Variable structure systems, including sliding mode approaches, are well known as very robust techniques. Sliding mode observers (SMO) have the same advantages of robustness upon uncertainty and disturbances as those of the SMC, but with the advantage that the so-called *chattering* effect is not present physically in the observed

[5] In the context of this paper, the UAV's approximated total mass and geometry can be useful to determine the numerical values of $\widetilde{\mathbf{\Xi}}(\mathbf{x}(t))$.

system [20]. The central idea of the SMO is that, given an uncertain nonlinear system the following form [21]

$$\begin{aligned}\dot{x}_1(t) &= x_2(t)\\ \dot{x}_2(t) &= x_3(t)\\ &\vdots\\ \dot{x}_n(t) &= f(\mathbf{x}(t), u(t)),\end{aligned}$$

with $\mathbf{x}(t) = \begin{bmatrix} x_1(t) & \cdots & x_n(t)\end{bmatrix}^T \in \mathbb{R}^n$, $u(t) \in \mathbb{R}$, and $f(\cdot,\cdot) \in \mathbb{R}$, it is possible to estimate its states using the single measurement available $x_1(t)$ by means of the following set of discontinuous functions

$$\begin{aligned}\dot{\hat{x}}_1(t) &= \lambda_1 e_1(t) + \hat{x}_2(t) + k_1 \text{sign}(e_1(t))\\ \dot{\hat{x}}_2(t) &= \lambda_2 e_1(t) + \hat{x}_3(t) + k_2 \text{sign}(e_1(t))\\ &\vdots\\ \dot{\hat{x}}_n(t) &= \lambda_n e_1(t) + \hat{f}(\mathbf{x}(t)) + u(t) + k_n \text{sign}(e_1(t))\end{aligned} \tag{6}$$

where $\hat{\mathbf{x}}(t) = \begin{bmatrix}\hat{x}_1(t) & \cdots & \hat{x}_n(t)\end{bmatrix}^T \in \mathbb{R}^n$ is the estimation state vector, $e_1(t) = x_1(t) - \hat{x}_1(t) \in \mathbb{R}$ is the observation error, $k_1,\ k_2,\ \ldots,\ k_n \in \mathbb{R}$ are tunable gains, and $\hat{f}(\cdot) \in \mathbb{R}$ is an average estimation of $f(\cdot,\cdot)$ produced by the high frequency sliding mode [21]. The constants $\lambda_i \in \mathbb{R}$, with $i = 1, \ldots, n$, determine the performance of the observer before the sliding mode occurs at $e_1 = 0$ [22]. The estimation $\hat{f}$ could be recovered and used within an ADRC scheme through an appropriate low-pass filtering stage. Nevertheless, such a stage would introduce phase lag, and the number of tuning parameters for the overall control-observer system would increase. Thus, the use of a sliding-mode extended-state observer (SMESO) is proposed in this work to robustly estimate the total disturbance (2) [20], exploiting the advantages of the SMO and the ESO, but avoiding the low pass filtering and linear observation drawbacks.

2.3. Stability and Ultimate Boundness Conditions for Perturbed Systems

This subsection addresses the problem of determining stability and ultimate bounds for exponentially stable nonlinear systems affected by vanishing and/or non vanishing perturbations. This is useful when part of the system dynamics is uncertain or is treated as a disturbance, for instance, when additive terms arise from a linearization [23,24]. Consider a nonlinear system with disturbances

$$\dot{\mathbf{x}} = \mathbf{f}(t, \mathbf{x}) + \mathbf{d}(t, \mathbf{x}) \tag{7}$$

where $\mathbf{x} \in \mathcal{D}$ is the state vector, $\mathcal{D} = \{\mathbf{x} \in \mathbb{R}^n, \|\mathbf{x}\| < \rho\}$, $\rho > 0$, $\mathbf{f}(t, \mathbf{x}) : [0, \infty) \times \mathcal{D} \to \mathbb{R}^n$ is the system dynamics and $\mathbf{d}(t, \mathbf{x}) : [0, \infty) \times \mathcal{D} \to \mathbb{R}^n$ contains the disturbances; both are locally Lipschitz in $\mathbf{x}$ and piecewise continuous in t. Such a representation is always possible for uncertainties that do not change the system's order [24]. Assuming that (7) has an asymptotically stable equilibrium in $\mathbf{x} = \mathbf{0}_n$, with $\mathbf{0}_n \in \mathbb{R}^n$ the zero vector of proper dimension, when $\mathbf{d}(t, \mathbf{x}) = \mathbf{0}_n$, the goal is to study whether the stability of (7) is affected when $\mathbf{d}(t, \mathbf{x}) \neq \mathbf{0}_n$. In this context, two cases may arise: $\mathbf{d}(t, \mathbf{x})$ is vanishing or non vanishing. In the former case, $\mathbf{d}(t, \mathbf{0}_n) = \mathbf{0}_n$, the equilibrium is still the origin; whereas, in the latter case, $\mathbf{d}(t, \mathbf{0}_n) \neq \mathbf{0}_n$, the equilibrium is not the origin anymore, but an ultimate bounded solution can be found [24]. The following result from the literature is useful to study the aforementioned stability problems.

Lemma 1. *[24, Chap. 5] Let the origin be an exponentially stable equilibrium of the system (7) with* $\mathbf{d}(t,\mathbf{x}) = \mathbf{0}_n$. *Let* $V(t,\mathbf{x})$ *be a Lyapunov function satisfying*

$$c_1\|\mathbf{x}\|^2 \leq V(t,\mathbf{x}) \leq c_2\|\mathbf{x}\|^2, \tag{8a}$$

$$\frac{\partial V}{\partial \mathbf{t}} + \frac{\partial V}{\partial \mathbf{x}}\mathbf{f}(t,\mathbf{x}) \leq -c_3\|\mathbf{x}\|^2, \tag{8b}$$

$$\left\|\frac{\partial V}{\partial \mathbf{x}}\right\| \leq c_4\|\mathbf{x}\|. \tag{8c}$$

Suppose now $\mathbf{d}(t,\mathbf{x}) \neq \mathbf{0}_n$ *and that there exist scalar constants* $c_6 > 0$ *and* $0 < c_7 < 1$ *such that*

$$\|\mathbf{d}(t,\mathbf{x})\| \leq c_6 < \frac{c_3}{c_4}\sqrt{\frac{c_1}{c_2}}c_7\rho, \ \forall\, t \geq 0, \ \forall\, \mathbf{x} \in \mathcal{D}. \tag{9}$$

Then, the solution $\mathbf{x}(t)$ *of (7) satisfies*

$$\|\mathbf{x}(t)\| \leq \sqrt{\frac{c_2}{c_1}}exp\left[-\frac{(1-c_7)c_3}{2c_2}(t-t_0)\right]\|\mathbf{x}(0)\|, \ \forall\, t_0 \leq t < t_1 \tag{10a}$$

and

$$\|\mathbf{x}(t)\| \leq \frac{c_4c_6}{c_3c_7}\sqrt{\frac{c_2}{c_1}}, \ \forall\, t \geq t_1. \tag{10b}$$

In other words, the solution $\mathbf{x}(t)$ *is uniformly ultimately bounded.*

Proof of Lemma 1. See Lemma 5.2 in [24]. □

2.4. Dynamics of omnidirectional multirotor UAVs

Consider a fixed world frame $\mathcal{F}_W = \boldsymbol{O}_W, \{\mathbf{x}_W, \mathbf{y}_W, \mathbf{z}_W\}$ and the body frame of the hexarotor $\mathcal{F}_b = \boldsymbol{O}_b, \{\mathbf{x}_b, \mathbf{y}_b, \mathbf{z}_b\}$ which is attached to its center of mass (CoM), and six coordinate frames $\mathcal{F}_{S_i} = \boldsymbol{O}_{S_i}, \{\mathbf{x}_{S_i}, \mathbf{y}_{S_i}, \mathbf{z}_{S_i}\}, i = 1, ..., 6$, attached to each propeller of the

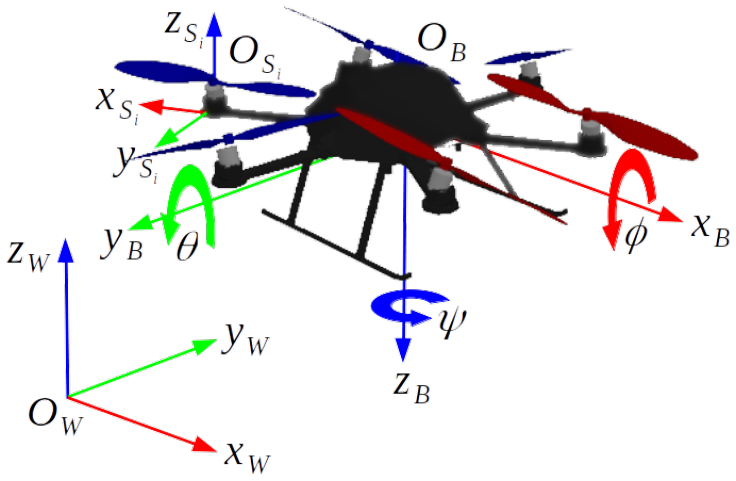

Figure 1. Hexarotor with tilted propellers and reference frames. O_W is the world reference frame and O_B is the airframe coordinate frame. O_{S_i} is the coordinate frame of the $i-$th propeller.

hexarotor [25]. All these frames are illustrated in Figure 1. The pose of the airframe respect to $\mathcal{F}_W$ is represented by

$$\mathbf{p}_b = \begin{bmatrix} x & y & z \end{bmatrix}^T \in \mathbb{R}^3, \tag{11a}$$

$$\boldsymbol{\eta}_b = \begin{bmatrix} \phi & \theta & \psi \end{bmatrix}^T \in \mathbb{R}^3, \tag{11b}$$

where $x, y, z \in \mathbb{R}$ are the translational motion Cartesian coordinates representing the position of $\mathcal{F}_b$ in $\mathcal{F}_W$ and $\phi, \theta, \psi \in \mathbb{R}$ are the Euler orientation angles about $\mathbf{x}_b$, $\mathbf{y}_b$, and $\mathbf{z}_b$, respectively. The orientation of $\mathcal{F}_b$ respect to $\mathcal{F}_W$ is given by the rotation matrix $\mathbf{R}_b \in \mathrm{SO}(3)$, whose expression is given below

$$\mathbf{R}_b(\boldsymbol{\eta}_b) = \begin{bmatrix} c_\psi c_\theta & c_\psi s_\theta s_\phi - s_\psi c_\phi & c_\psi s_\theta c_\phi + s_\psi s_\phi \\ s_\psi c_\theta & s_\psi s_\theta s_\phi + c_\psi c_\phi & s_\psi s_\theta c_\phi - c_\psi s_\phi \\ -s_\theta & c_\theta s_\phi & c_\theta c_\phi \end{bmatrix}, \tag{12}$$

where $c_{(\cdot)} \triangleq \cos(\cdot)$ and $s_{(\cdot)} \triangleq \sin(\cdot)$. Let $\dot{\mathbf{p}}_b \in \mathbb{R}^3$ denote the absolute translational velocity of the UAV expressed in $\mathcal{F}_W$, while $\dot{\boldsymbol{\eta}}_b \in \mathbb{R}^3$ is the time derivative of $\boldsymbol{\eta}_b$. Then, the dynamics of an omnidirectional multirotor UAV can be written as [26]:

$$m\ddot{\mathbf{p}}_b = mg\mathbf{e}_3 + \mathbf{R}_b(\boldsymbol{\eta}_b)\mathbf{u}_f + \mathbf{f}_u(\cdot), \tag{13a}$$

$$\mathbf{M}(\boldsymbol{\eta}_b)\ddot{\boldsymbol{\eta}}_b = -\mathbf{C}(\boldsymbol{\eta}_b, \dot{\boldsymbol{\eta}}_b)\dot{\boldsymbol{\eta}}_b + \boldsymbol{\Omega}(\boldsymbol{\eta}_b)^T\mathbf{u}_\tau + \boldsymbol{\tau}_u(\cdot), \tag{13b}$$

where $m > 0$ is a scalar denoting the total mass of the UAV, g is a scalar representing the gravity acceleration, $\mathbf{e}_3 = [0\ 0\ 1]^T$, $\mathbf{u}_f,\ \mathbf{u}_\tau \in \mathbb{R}^3$ are the control forces and torques vectors respectively, $\mathbf{f}_u(\cdot),\ \boldsymbol{\tau}_u(\cdot) \in \mathbb{R}^3$ represent the external forces and torques respectively,

$$\boldsymbol{\Omega}(\boldsymbol{\eta}_b) = \begin{bmatrix} 1 & 0 & -s_\theta \\ 0 & c_\phi & c_\theta s_\phi \\ 0 & -s_\phi & c_\theta c_\phi \end{bmatrix},$$

$\mathbf{M}(\boldsymbol{\eta}_b) \in \mathbb{R}^{3\times3} = \boldsymbol{\Omega}(\boldsymbol{\eta}_b)^T\boldsymbol{I}_b\boldsymbol{\Omega}(\boldsymbol{\eta}_b)$ with $\boldsymbol{I}_b \in \mathbb{R}^{3\times3}$ representing the inertia tensor of the UAV and

$$\mathbf{C}(\boldsymbol{\eta}_b, \dot{\boldsymbol{\eta}}_b) \in \mathbb{R}^{3\times3} = \boldsymbol{\Omega}(\boldsymbol{\eta}_b)^T[\boldsymbol{\Omega}(\boldsymbol{\eta}_b)\dot{\boldsymbol{\eta}}_b]_\times\boldsymbol{I}_b\boldsymbol{\Omega}(\boldsymbol{\eta}_b) + \boldsymbol{\Omega}(\boldsymbol{\eta}_b)^T\boldsymbol{I}_b\dot{\boldsymbol{\Omega}}(\boldsymbol{\eta}_b),$$

with $[\cdot]_\times$ denoting the skew symmetric matrix. Considering the state $\bar{\mathbf{x}} = [\underbrace{\mathbf{p}_b^T\ \boldsymbol{\eta}_b^T}_{\mathbf{x}_1}\ \underbrace{\dot{\mathbf{p}}_b^T\ \dot{\boldsymbol{\eta}}_b^T}_{\mathbf{x}_2}]^T$, the dynamics (13a)–(13b) can be rewritten as:

$$\dot{\bar{\mathbf{x}}} = \mathbf{A}\bar{\mathbf{x}} + \mathbf{B}\mathbf{u} + \begin{bmatrix} \mathbf{0}_6 \\ \boldsymbol{\delta}_1(\boldsymbol{\eta}_b, \dot{\boldsymbol{\eta}}_b, g) + \boldsymbol{\delta}_2(\cdot) \end{bmatrix}, \tag{14}$$

where

$$\mathbf{A} \in \mathbb{R}^{12\times12} \triangleq \begin{bmatrix} \mathbf{O}_{6\times6} & \mathbf{I}_{6\times6} \\ \mathbf{O}_{6\times6} & \mathbf{O}_{6\times6} \end{bmatrix}, \qquad \mathbf{B} \in \mathbb{R}^{12\times6} \triangleq \underbrace{\begin{bmatrix} \underbrace{\boldsymbol{O}_{6\times6}}_{\mathbf{B}_1} \\ \begin{bmatrix} m\mathbf{I}_{3\times3} & \boldsymbol{O}_{3\times3} \\ \boldsymbol{O}_{3\times3} & \mathbf{M}(\boldsymbol{\eta}_b) \end{bmatrix}^{-1}\begin{bmatrix} \mathbf{R}_b(\boldsymbol{\eta}_b) & \boldsymbol{O}_{3\times3} \\ \boldsymbol{O}_{3\times3} & \boldsymbol{\Omega}(\boldsymbol{\eta}_b) \end{bmatrix} \end{bmatrix}}_{\mathbf{B}_2},$$

where $\boldsymbol{O}_{n\times m} \in \mathbb{R}^{n\times m}$ is the zero matrix of proper dimensions, $\boldsymbol{I}_{n\times m} \in \mathbb{R}^{n\times m}$ is the identity matrix of proper dimensions, $\mathbf{u} = [\mathbf{u}_f^T\ \mathbf{u}_\tau^T]^T$ is a six-dimensional control vector,

$$\boldsymbol{\delta}_1(\boldsymbol{\eta}_b, \dot{\boldsymbol{\eta}}_b, g) \in \mathbb{R}^6 \triangleq \mathbf{B}_2^{-1}\begin{bmatrix} -g\mathbf{e}_3^T & (-\mathbf{C}(\boldsymbol{\eta}_b, \dot{\boldsymbol{\eta}}_b)\dot{\boldsymbol{\eta}}_b)^T \end{bmatrix}^T \tag{15}$$

is the vector containing gravity and Coriolis effects (that is considered as a disturbance term), and $\boldsymbol{\delta}_2(\cdot) \in \mathbb{R}^6 \triangleq \left[\mathbf{f}_u(\cdot)^T \ \boldsymbol{\tau}_u(\cdot)^T\right]^T$ is the lumped vector of disturbances, including both external effects and the net term caused by parametric uncertainty. The term $\boldsymbol{\delta}_2(\cdot)$ is typically unknown but bounded, $\|\boldsymbol{\delta}_2(\cdot)\| \leq \gamma_{\delta_2} < +\infty$, and differentiable or at least with a removable discontinuity such that its time derivative is also bounded, $\|\dot{\boldsymbol{\delta}}_2(\cdot)\| \leq \gamma_{\dot{\delta}_2} < +\infty$. The following assumptions can also be done about (14):

A1. The aerial vehicle does not pass through singularities [26]. Besides, it moves using the thrust incoming from the tilted propellers rather than changing its orientation to generate a thrust to move horizontally. In addition, it takes off in with zero *roll* and *pitch*, and it is desired to maintain such values. Thus, the matrix $\mathbf{B}_2$ can be considered invertible.

A2. Since $\mathbf{B}_2$ is invertible within some range and its norm is bounded[6], then $\mathbf{C}(\boldsymbol{\eta}, \dot{\boldsymbol{\eta}})$ is Lipschitz continuous and it does not grow faster than its arguments [27]. Hence, the following bounds hold

$$\|\boldsymbol{\delta}_1(\boldsymbol{\eta}_b, \dot{\boldsymbol{\eta}}_b, g)\| \leq \gamma_{\delta_1} \tag{16}$$
$$\|\dot{\boldsymbol{\delta}}_1(\boldsymbol{\eta}_b, \dot{\boldsymbol{\eta}}_b, g)\| \leq \gamma_{\dot{\delta}_1}, \tag{17}$$

with $\gamma_{\delta_1}, \gamma_{\dot{\delta}_1} > 0$.

3. Controller Design

3.1. Control problem

Consider the passively-tilted hexarotor dynamics (14). The control problem is to lead $[\mathbf{x}_1^T \ \mathbf{x}_2^T]^T \in \mathbb{R}^{12}$ to the desired set-point or trajectory $[\mathbf{x}_1^{dT} \ \mathbf{x}_2^{dT}]^T \in \mathbb{R}^{12}$ despite the affecting disturbances. An appropriate solution is

$$\mathbf{u} = \mathbf{B}_2^{-1}[\mathbf{v} - \boldsymbol{\delta}_1(\boldsymbol{\eta}_b, \dot{\boldsymbol{\eta}}_b, g) - \boldsymbol{\delta}_2(\cdot)], \tag{18}$$

where $\mathbf{v} \in \mathbb{R}^6$ is a virtual linear control input that can be shaped through any pole placement technique, for instance

$$\mathbf{v} = \mathbf{K}\begin{bmatrix}\tilde{\mathbf{x}}_1 \\ \tilde{\mathbf{x}}_2\end{bmatrix}, \tag{19}$$

where

$$\begin{bmatrix}\tilde{\mathbf{x}}_1 \\ \tilde{\mathbf{x}}_2\end{bmatrix} \in \mathbb{R}^{12} = \begin{bmatrix}\mathbf{x}_1^d \\ \mathbf{x}_2^d\end{bmatrix} - \begin{bmatrix}\mathbf{x}_1 \\ \mathbf{x}_2\end{bmatrix}$$

is the error signal and $\mathbf{K} \in \mathbb{R}^{6\times 12}$ is a constant gain matrix. For the ideal case when the dynamics of the UAV are completely known, all the states are measurable and the external disturbances are absent (i.e., $\dot{\boldsymbol{\delta}}_2(\cdot) = \mathbf{0}_6$), the controller (18) is enough to solve the control problem, since $\boldsymbol{\delta}_1(\boldsymbol{\eta}_b, \dot{\boldsymbol{\eta}}_b, g)$ is also known. On the other hand, external disturbances $\boldsymbol{\delta}_2(\cdot)$ are usually unknown but bounded. Hence, when the UAV is affected by them, a control action to compensate for their effect is required. Below, rejecting disturbances affecting (14) is explained: the technique consists of estimating and compensating online the total disturbance using a robust extended-state observer. The following two cases are presented: the former considers the external disturbance rejection via an extended-state observer and perfect cancellation of $\boldsymbol{\delta}_1(\cdot)$; in the latter, such a vector is estimated as well.

3.2. External Disturbances Rejection Via Extended-State Observer and Perfect Cancellation of System Nonlinearities

Usually, the ADRC theory requests the knowledge of some boundaries for the total disturbance lumped within an additional state from the original system. In such a case,

[6] Such a matrix is composed of the mass matrix, which is bounded for mechanical systems, a rotation matrix and $\boldsymbol{\Omega}(\cdot)$ whose norms are bounded because they are composed of sines and cosines terms.

several types of extended-state observers have been implemented, including, recently, sliding mode approaches. For the case of the passively tilted hexarotors, this theory has not been applied. The closest works are about ADRC applied to coplanar (non-tilted) hexarotors [3,4], but the convergence of the observers is missing. Below, the convergence of sliding-mode extended-state observer and the ADRC based on such an observation technique are presented. For control design, the fully actuated multirotor UAV subjected to external disturbances in (14) can be rewritten in the following extended-state form

$$\begin{cases} \dot{\mathbf{x}}_1 = \mathbf{x}_2, \\ \dot{\mathbf{x}}_2 = \mathbf{B}_2\mathbf{u} + \delta_1(\boldsymbol{\eta}_b, \dot{\boldsymbol{\eta}}_b, g) + \mathbf{x}_3, \\ \dot{\mathbf{x}}_3 = \dot{\delta}_2(\cdot). \end{cases} \tag{20}$$

Assuming an accurate knowledge of the parameters of the UAV dynamics (20) and an accurate measure of $\mathbf{x}_1$ and $\mathbf{x}_2$[7], a controller that satisfies set-point regulation and tracking is the following ADRC

$$\mathbf{u} = \mathbf{B}_2^{-1}\left[\mathbf{v} - \delta_1(\boldsymbol{\eta}_b, \dot{\boldsymbol{\eta}}_b, g) - \hat{\mathbf{x}}_3 + \dot{\mathbf{x}}_2^d\right], \tag{21}$$

from which $\hat{\mathbf{x}}_3$ can be retrieved through the following robust SMESO

$$\begin{cases} \dot{\hat{\mathbf{x}}}_1 = & \hat{\mathbf{x}}_2 + \varepsilon^{-1}(\mathbf{x}_1 - \hat{\mathbf{x}}_1) + k_1\text{sign}(\mathbf{x}_1 - \hat{\mathbf{x}}_1) \\ \dot{\hat{\mathbf{x}}}_2 = & \hat{\mathbf{x}}_3 + \varepsilon^{-2}(\mathbf{x}_1 - \hat{\mathbf{x}}_1) + k_2\text{sign}(\mathbf{x}_1 - \hat{\mathbf{x}}_1) + \mathbf{B}_2\mathbf{u} + \delta_1(\boldsymbol{\eta}_b, \dot{\boldsymbol{\eta}}_b, g) \\ \dot{\hat{\mathbf{x}}}_3 = & \varepsilon^{-3}(\mathbf{x}_1 - \hat{\mathbf{x}}_1) + k_3\text{sign}(\mathbf{x}_1 - \hat{\mathbf{x}}_1), \end{cases} \tag{22}$$

where $\hat{\mathbf{x}}_i \in \mathbb{R}^6$ contains the estimation of $\mathbf{x}_i$, $0 < \varepsilon \ll 1$ is a scalar such that the polynomial $s^3 + \varepsilon^{-1}s^2 + \varepsilon^{-2}s + \varepsilon^{-3}$ is Hurwitz, and k_1, k_2, k_3 are positive scalars satisfying $\varepsilon^{-1} > k_3 > k_2 > k_1 > \gamma_{\dot{\delta}_2}$.

The boundedness of the estimation and the tracking errors are now shown in the following theorems.

Theorem 1. *The external disturbances $\delta_2(\cdot)$ are accurately reconstructed by the extended robust SMESO (22), i.e., the observation error $\tilde{\hat{\mathbf{x}}} = \mathbf{x} - \hat{\mathbf{x}} \in \mathbb{R}^{18}$ is uniformly ultimately bounded.*

Proof of Theorem 1. Considering (20), the dynamics of the SMESO (22) is

$$\dot{\tilde{\hat{\mathbf{x}}}} \triangleq \begin{bmatrix} \dot{\tilde{\hat{\mathbf{x}}}}_1 \\ \dot{\tilde{\hat{\mathbf{x}}}}_2 \\ \dot{\tilde{\hat{\mathbf{x}}}}_3 \end{bmatrix} = \underbrace{\begin{bmatrix} -\varepsilon^{-1}\mathbf{I}_{6\times6} & \mathbf{I}_{6\times6} & \mathbf{0}_{6\times6} \\ -\varepsilon^{-2}\mathbf{I}_{6\times6} & \boldsymbol{O}_{6\times6} & \mathbf{I}_{6\times6} \\ -\varepsilon^{-3}\mathbf{I}_{6\times6} & \boldsymbol{O}_{6\times6} & \boldsymbol{O}_{6\times6} \end{bmatrix}}_{\tilde{\mathbf{A}}} \underbrace{\begin{bmatrix} \tilde{\hat{\mathbf{x}}}_1 \\ \tilde{\hat{\mathbf{x}}}_2 \\ \tilde{\hat{\mathbf{x}}}_3 \end{bmatrix}}_{\tilde{\hat{\mathbf{x}}}} - \underbrace{\begin{bmatrix} k_1\mathbf{I}_{6\times6} & \boldsymbol{O}_{6\times6} & \boldsymbol{O}_{6\times6} \\ \boldsymbol{O}_{6\times6} & k_2\mathbf{I}_{6\times6} & \boldsymbol{O}_{6\times6} \\ \boldsymbol{O}_{6\times6} & \boldsymbol{O}_{6\times6} & k_3\mathbf{I}_{6\times6} \end{bmatrix}}_{\mathbf{K_O}} \text{sign}(\tilde{\hat{\mathbf{x}}}_1) + \underbrace{\begin{bmatrix} \boldsymbol{O}_{6\times6} \\ \boldsymbol{O}_{6\times6} \\ \mathbf{I}_{6\times6} \end{bmatrix}}_{\mathbf{D}_1} \dot{\delta}_2(\cdot).$$

Considering the linear system $\dot{\tilde{\hat{\mathbf{x}}}} = \tilde{\mathbf{A}}\tilde{\hat{\mathbf{x}}}$, since $\tilde{\mathbf{A}}$ is Hurwitz, there exists a symmetric positive definite matrix $\tilde{\mathbf{P}}_1 \in \mathbb{R}^{18\times18}$ such that $\tilde{\mathbf{A}}^T\tilde{\mathbf{P}}_1 + \tilde{\mathbf{P}}_1\tilde{\mathbf{A}} = -2\mathbf{I}_{18\times18}$ and hence, a candidate Lyapunov function $V_1(\tilde{\hat{\mathbf{x}}}) = \tilde{\hat{\mathbf{x}}}^T\tilde{\mathbf{P}}_1\tilde{\hat{\mathbf{x}}}$ can be proposed. Notice that such a function satisfies (8a)

$$\lambda_{\min}(\tilde{\mathbf{P}}_1)\|\mathbf{x}\|^2 \leq V_1(\tilde{\hat{\mathbf{x}}}) \leq \lambda_{\max}(\tilde{\mathbf{P}}_1)\|\mathbf{x}\|^2.$$

Besides, the conditions (8b) and (8c) are satisfied with $c_3 = 2$ and $c_4 = 2\lambda_{\max}(\tilde{\mathbf{P}}_1)$, respectively.

[7] The vector $\mathbf{x}_2$ could be, in principle, estimated.

Now, considering the full system $\dot{\hat{\tilde{\mathbf{x}}}} = \tilde{\mathbf{A}}\hat{\tilde{\mathbf{x}}} - \mathbf{K}_o \text{sign}(\hat{\tilde{\mathbf{x}}}_1) + \mathbf{D}_1\dot{\delta}_2(\cdot)$, Lemma 1 must be followed with the position $\rho = +\infty$. Therefore, the following ultimate bound can be proved

$$\|\mathbf{K}_o \text{sign}(\hat{\tilde{\mathbf{x}}}_1) + \mathbf{D}_1\dot{\delta}_2(\cdot)\| \leq \sqrt{6}k_3 + \gamma_{\dot{\delta}_2} < +\infty.$$

Hence, the solution of the SMESO system satisfies the following bounds

$$\|\hat{\tilde{\mathbf{x}}}(t)\| \leq \begin{cases} \sqrt{\dfrac{\lambda_{\max}(\tilde{\mathbf{P}}_1)}{\lambda_{\min}(\tilde{\mathbf{P}}_1)}} \exp\left[-\dfrac{(1-\vartheta_1)}{\lambda_{\max}(\tilde{\mathbf{P}}_1)}(t-t_0)\right] \|\hat{\tilde{\mathbf{x}}}(0)\|, \ \forall\, t_0 \leq t < t_1 \\ \\ b_1, \ \forall\, t \geq t_1, \end{cases}$$

with $0 < \vartheta_1 < 1$ and where

$$b_1 = \frac{\lambda_{\max}(\tilde{\mathbf{P}}_1)\left[\gamma_{\dot{\delta}_2} + \sqrt{6}k_3\right]}{\vartheta_1} \sqrt{\frac{\lambda_{\max}(\tilde{\mathbf{P}}_1)}{\lambda_{\min}(\tilde{\mathbf{P}}_1)}}.$$

Notice that the gain k_3 is helpful to reduce the ultimate bound for the solutions of $\hat{\tilde{\mathbf{x}}}$. □

Theorem 2. *The error vector* $[\tilde{\mathbf{x}}_1^T \ \tilde{\mathbf{x}}_2^T]^T \in \mathbb{R}^{12} \triangleq [\mathbf{x}_1^{dT} \ \mathbf{x}_2^{dT}]^T - [\mathbf{x}_1^T \ \mathbf{x}_2^T]^T$, *with* $\dot{\mathbf{x}}_1^d = \mathbf{x}_2^d$, *is uniformly ultimate bounded by means of the controller* (21).

Proof of Theorem 2. Considering (20), the tracking error dynamics is

$$\begin{cases} \dot{\tilde{\mathbf{x}}}_1 = \tilde{\mathbf{x}}_2, \\ \dot{\tilde{\mathbf{x}}}_2 = \dot{\mathbf{x}}_2^d - \mathbf{B}_2\mathbf{u} - \delta_1(\boldsymbol{\eta}_b, \dot{\boldsymbol{\eta}}_b, g) - \mathbf{x}_3. \end{cases}$$

Substituting the controller (21) into the error dynamics yields

$$\begin{cases} \dot{\tilde{\mathbf{x}}}_1 = \tilde{\mathbf{x}}_2, \\ \dot{\tilde{\mathbf{x}}}_2 = -\mathbf{v} + \hat{\mathbf{x}}_3 - \mathbf{x}_3. \end{cases}$$

Considering $\hat{\mathbf{x}}_3 - \mathbf{x}_3 = -\hat{\tilde{\mathbf{x}}}_3$ then,

$$\begin{bmatrix} \dot{\tilde{\mathbf{x}}}_1 \\ \dot{\tilde{\mathbf{x}}}_2 \end{bmatrix} = \begin{bmatrix} \boldsymbol{O}_{6\times6} & \mathbf{I}_{6\times6} \\ \boldsymbol{O}_{6\times6} & \boldsymbol{O}_{6\times6} \end{bmatrix} \begin{bmatrix} \tilde{\mathbf{x}}_1 \\ \tilde{\mathbf{x}}_2 \end{bmatrix} - \begin{bmatrix} \boldsymbol{O}_{6\times6} \\ \mathbf{I}_{6\times6} \end{bmatrix} \mathbf{v} - \begin{bmatrix} \boldsymbol{O}_{6\times6} \\ \mathbf{I}_{6\times6} \end{bmatrix} \hat{\tilde{\mathbf{x}}}_3.$$

Folding (18) into the last expression yields

$$\begin{bmatrix} \dot{\tilde{\mathbf{x}}}_1 \\ \dot{\tilde{\mathbf{x}}}_2 \end{bmatrix} = \mathbf{A}_1 \begin{bmatrix} \tilde{\mathbf{x}}_1 \\ \tilde{\mathbf{x}}_2 \end{bmatrix} - \begin{bmatrix} \boldsymbol{O}_{6\times6} \\ \mathbf{I}_{6\times6} \end{bmatrix} \hat{\tilde{\mathbf{x}}}_3,$$

with

$$\mathbf{A}_1 = \begin{bmatrix} \boldsymbol{O}_{6\times6} & \mathbf{I}_{6\times6} \\ \boldsymbol{O}_{6\times6} & \boldsymbol{O}_{6\times6} \end{bmatrix} - \begin{bmatrix} \boldsymbol{O}_{6\times6} \\ \mathbf{I}_{6\times6} \end{bmatrix} \mathbf{K},$$

and such that $\mathbf{K}$ makes $\mathbf{A}_1$ Hurwitz.

Considering the nominal linear system with $\hat{\tilde{\mathbf{x}}}_3 = \mathbf{0}_6$, a candidate Lyapunov function $V_2(\tilde{\mathbf{x}}_1, \tilde{\mathbf{x}}_2) = [\tilde{\mathbf{x}}_1^T \ \tilde{\mathbf{x}}_2^T]^T \mathbf{P}_1 [\tilde{\mathbf{x}}_1^T \ \tilde{\mathbf{x}}_2^T]$ can be proposed, where $\mathbf{P}_1 \in \mathbb{R}^{12\times12}$ is a symmetric positive definite matrix which is solution of

$$\mathbf{A}_1^T\mathbf{P}_1 + \mathbf{P}_1\mathbf{A_1} = -2\mathbf{I}_{12\times12}.$$

Notice that such a function satisfies (8a)

$$\lambda_{\min}(\mathbf{P}_1)\|\mathbf{x}\|^2 \leq V_2(\hat{\tilde{\mathbf{x}}}) \leq \lambda_{\max}(\mathbf{P}_1)\|\mathbf{x}\|^2.$$

Besides, the conditions (8b) and (8c) are satisfied with $c_3 = 2$ and $c_4 = 2\lambda_{\max}(\mathbf{P}_1)$, respectively. Besides, the conditions (8b) and (8c) are satisfied with $c_3 = 2$ and $c_4 = 2\lambda_{\max}(\tilde{\mathbf{P}}_1)$, respectively.

Now, considering the full system with the generic condition $\hat{\tilde{\mathbf{x}}}_3 \neq \mathbf{0}_6$, Lemma 1 must be followed with the position $\rho = +\infty$. The ultimate bound for $\hat{\tilde{\mathbf{x}}}_3$ can be retrieved from Theorem 1. Thus, the solutions of the tracking error dynamics is uniformly ultimate bounded by

$$\left\| \begin{bmatrix} \tilde{\mathbf{x}}_1(t) \\ \tilde{\mathbf{x}}_2(t) \end{bmatrix} \right\| \leq \begin{cases} \sqrt{\dfrac{\lambda_{\max}(\mathbf{P}_1)}{\lambda_{\min}(\mathbf{P}_1)}} \exp\left[-\dfrac{(1-\vartheta_2)}{\lambda_{\max}(\mathbf{P}_1)}(t-t_0) \right] \left\| \begin{bmatrix} \tilde{\mathbf{x}}_1(0) \\ \tilde{\mathbf{x}}_2(0) \end{bmatrix} \right\|, \ \forall\, t_0 \leq t < t_2 \\ \\ b_2, \ \forall\, t \geq t_2, \end{cases}$$

where

$$b_2 = \frac{b_1 \lambda_{\max}(\mathbf{P}_1)}{\vartheta_2} \sqrt{\frac{\lambda_{\max}(\mathbf{P}_1)}{\lambda_{\min}(\mathbf{P}_1)}},$$

and $t_2 > t_1$. Notice that the ultimate bound b_2 depends directly on b_1. □

3.3. Robust External Disturbances Rejection Via Extended-State Observer

In case these disturbances are differentiable in its arguments, locally Lipschitz, or at least have a removable discontinuity (for the case of external disturbances), an augmented-state representation for (14) can be used as follows

$$\dot{\mathbf{x}} \triangleq \begin{cases} \dot{\mathbf{x}}_1 = \mathbf{x}_2 \\ \dot{\mathbf{x}}_2 = \mathbf{B}_2\mathbf{u} + \mathbf{x}_3 \\ \dot{\mathbf{x}}_3 = \dot{\delta}_1(\boldsymbol{\eta}_b, \dot{\boldsymbol{\eta}}_b, g) + \dot{\delta}_2(\cdot). \end{cases} \tag{23}$$

A controller that satisfies set-point regulation and tracking is the following ADRC

$$\mathbf{u} = \mathbf{B}_2^{-1}\left[\mathbf{v} - \hat{\mathbf{x}}_3 + \dot{\mathbf{x}}_2^d \right], \tag{24}$$

where $\mathbf{v}$ is the same as in (19). The difference with respect to (21) is the missing compensation for the term $\delta_1(\cdot)$. The estimate of $\hat{\mathbf{x}}_3$ can be retrieved through the following robust SMESO

$$\begin{cases} \dot{\hat{\mathbf{x}}}_1 = & \hat{\mathbf{x}}_2 + \varepsilon^{-1}(\mathbf{x}_1 - \hat{\mathbf{x}}_1) + k_1 \text{sign}(\mathbf{x}_1 - \hat{\mathbf{x}}_1), \\ \dot{\hat{\mathbf{x}}}_2 = & \hat{\mathbf{x}}_3 + \varepsilon^{-2}(\mathbf{x}_1 - \hat{\mathbf{x}}_1) + k_2 \text{sign}(\mathbf{x}_1 - \hat{\mathbf{x}}_1) + \mathbf{B}_2\mathbf{u}, \\ \dot{\hat{\mathbf{x}}}_3 = & \varepsilon^{-3}(\mathbf{x}_1 - \hat{\mathbf{x}}_1) + k_3 \text{sign}(\mathbf{x}_1 - \hat{\mathbf{x}}_1). \end{cases} \tag{25}$$

The boundedness of the estimation and the tracking errors are now shown in the following theorems.

Theorem 3. *The disturbances of* (20) *are accurately reconstructed by the extended robust SMESO* (25) *despite the missing compensation for* $\delta_1(\boldsymbol{\eta}_b, \dot{\boldsymbol{\eta}}_b, g)$*, i.e., the observation error* $\hat{\tilde{\mathbf{x}}} = \mathbf{x} - \hat{\mathbf{x}} \in \mathbb{R}^{18\times 18}$ *is uniformly ultimately bounded.*

Proof of Theorem 3. Considering (23), the dynamics of the SMESO (25) is

$$\dot{\hat{\tilde{\mathbf{x}}}} \triangleq \begin{bmatrix} \dot{\hat{\tilde{\mathbf{x}}}}_1 \\ \dot{\hat{\tilde{\mathbf{x}}}}_2 \\ \dot{\hat{\tilde{\mathbf{x}}}}_3 \end{bmatrix} = \underbrace{\begin{bmatrix} -\varepsilon^{-1}\mathbf{I}_{6\times6} & \mathbf{I}_{6\times6} & \boldsymbol{O}_{6\times6} \\ -\varepsilon^{-2}\mathbf{I}_{6\times6} & \boldsymbol{O}_{6\times6} & \mathbf{I}_{6\times6} \\ -\varepsilon^{-3}\mathbf{I}_{6\times6} & \boldsymbol{O}_{6\times6} & \boldsymbol{O}_{6\times6} \end{bmatrix}}_{\tilde{\mathbf{A}}} \underbrace{\begin{bmatrix} \hat{\tilde{\mathbf{x}}}_1 \\ \hat{\tilde{\mathbf{x}}}_2 \\ \hat{\tilde{\mathbf{x}}}_3 \end{bmatrix}}_{\hat{\tilde{\mathbf{x}}}} - \underbrace{\begin{bmatrix} k_1\mathbf{I}_{6\times6} & \boldsymbol{O}_{6\times6} & \boldsymbol{O}_{6\times6} \\ \boldsymbol{O}_{6\times6} & k_2\mathbf{I}_{6\times6} & \boldsymbol{O}_{6\times6} \\ \boldsymbol{O}_{6\times6} & \boldsymbol{O}_{6\times6} & k_3\mathbf{I}_{6\times6} \end{bmatrix}}_{\mathbf{K_O}} \text{sign}(\hat{\tilde{\mathbf{x}}}_1)$$
$$+ \underbrace{\begin{bmatrix} \boldsymbol{O}_{6\times6} \\ \boldsymbol{O}_{6\times6} \\ \mathbf{I}_{6\times6} \end{bmatrix}}_{\mathbf{D}_1} (\dot{\delta}_1(g, \boldsymbol{\eta}_b, \dot{\boldsymbol{\eta}}_b) + \dot{\delta}_2(\cdot)).$$

Considering the linear system $\dot{\hat{\tilde{\mathbf{x}}}} = \tilde{\mathbf{A}}\hat{\tilde{\mathbf{x}}}$, since $\tilde{\mathbf{A}}$ is Hurwitz, there exists a symmetric positive definite matrix $\tilde{\mathbf{P}}_2 \in \mathbb{R}^{18\times18}$ such that $\tilde{\mathbf{A}}^T\tilde{\mathbf{P}}_2 + \tilde{\mathbf{P}}_2\tilde{\mathbf{A}} = -2\mathbf{I}_{18\times18}$ and hence, a candidate Lyapunov function $V_3(\hat{\tilde{\mathbf{x}}}) = \hat{\tilde{\mathbf{x}}}^T\tilde{\mathbf{P}}_2\hat{\tilde{\mathbf{x}}}$ can be proposed. Notice that such a function satisfies (8a)

$$\lambda_{\min}(\tilde{\mathbf{P}}_2)\|\mathbf{x}\|^2 \leq V_3(\hat{\tilde{\mathbf{x}}}) \leq \lambda_{\max}(\tilde{\mathbf{P}}_2)\|\mathbf{x}\|^2.$$

Besides, the conditions (8b) and (8c) are satisfied with $c_3 = 2$ and $c_4 = 2\lambda_{\max}(\tilde{\mathbf{P}}_2)$, respectively.

Now, considering the full system

$$\dot{\hat{\tilde{\mathbf{x}}}} = \tilde{\mathbf{A}}\hat{\tilde{\mathbf{x}}} - \mathbf{K}_o\text{sign}(\hat{\tilde{\mathbf{x}}}_1) + \mathbf{D}_1(\dot{\delta}_1(\boldsymbol{\eta}_b, \dot{\boldsymbol{\eta}}_b) + \dot{\delta}_2(\cdot)),$$

Lemma 1 must be followed with the position $\rho = +\infty$. Therefore, taking into account (15) and A2, the following ultimate bound can be proved

$$\| - \mathbf{K}_o\text{sign}(\hat{\tilde{\mathbf{x}}}_1) + \mathbf{D}_1(\dot{\delta}_1(\boldsymbol{\eta}_b, \dot{\boldsymbol{\eta}}_b) + \dot{\delta}_2(\cdot))\| \leq \sqrt{6}k_3 + \gamma_{\dot{\delta}_1} + \gamma_{\dot{\delta}_2} < +\infty.$$

Hence, the solution of the SMESO system satisfies the following bounds

$$\|\hat{\tilde{\mathbf{x}}}(t)\| \leq \begin{cases} \sqrt{\dfrac{\lambda_{\max}(\tilde{\mathbf{P}}_2)}{\lambda_{\min}(\tilde{\mathbf{P}}_2)}}\exp\left[-\dfrac{(1-\vartheta_3)}{\lambda_{\max}(\tilde{\mathbf{P}}_2)}(t-t_0)\right]\|\hat{\tilde{\mathbf{x}}}(0)\|, \ \forall\, t_0 \leq t < t_1 \\ b_3, \ \forall\, t \geq t_1, \end{cases}$$

with $0 < \theta_3 < 1$ where

$$b_3 = \frac{\lambda_{\max}(\tilde{\mathbf{P}}_2)\left[\sqrt{6}k_3 + \gamma_{\dot{\delta}_1} + \gamma_{\dot{\delta}_2}\right]}{\vartheta_3}\sqrt{\frac{\lambda_{\max}(\tilde{\mathbf{P}}_2)}{\lambda_{\min}(\tilde{\mathbf{P}}_2)}}..$$

□

Theorem 4. *The error vector* $[\tilde{\mathbf{x}}_1^T \ \tilde{\mathbf{x}}_2^T]^T$ *is uniformly ultimately bounded by means of the controller* (24).

Proof of the Theorem 4. Considering (23), the tracking error dynamics is

$$\begin{cases} \dot{\tilde{\mathbf{x}}}_1 = \tilde{\mathbf{x}}_2, \\ \dot{\tilde{\mathbf{x}}}_2 = \dot{\mathbf{x}}_2^d - \mathbf{B}_2\mathbf{u} - \mathbf{x}_3. \end{cases}$$

Substituting the controller (24) yields

$$\begin{cases} \dot{\tilde{\mathbf{x}}}_1 = \tilde{\mathbf{x}}_2, \\ \dot{\tilde{\mathbf{x}}}_2 = -\mathbf{v} - \hat{\tilde{\mathbf{x}}}_3. \end{cases}$$

The procedure follows the proof within Theorem 2 and it is not reported here for brevity. However, it is worth noting that the ultimate bound for $\left|\left|\begin{bmatrix}\tilde{\mathbf{x}}_1(t)\\ \tilde{\mathbf{x}}_2(t)\end{bmatrix}\right|\right|$ now depends on b_3 from Theorem 3.

□

4. Controller Implementation

4.1. Control allocation

Consider the Figure 2, where the top and frontal views of the tilted multirotor with six actuators are presented. The position of the i-th propeller in $\mathcal{F}_B$ can be expressed mathematically as follows [28]

$$\mathbf{p}_{S_i}^b = L\mathbf{R}_z(\zeta_i)\begin{bmatrix}1 & 0 & 0\end{bmatrix}^T, \tag{26}$$

where $i = 1, ..., n$ depending on the multirotor, $L > 0$ is the distance between $\boldsymbol{O}_{S_i}$ and

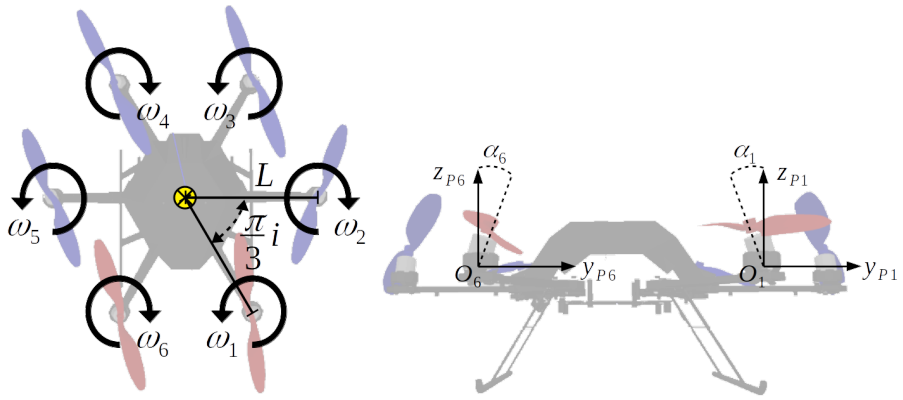

Figure 2. Left: Top view of the tilted hexarotor indicating each rotor spin direction, ω_i, the length L from the CoM of the airframe to the centre of rotation of a rotor, and in this case, $\zeta_i = \pi/3$. All the rotors are equidistant with respect to the CoM and the location angle of each rotor respect to the last one is the same. Right: Front view of the hexarotor showing two examples of the tilting angles. All the six rotors are tilted in the same magnitude but in different sense.

$\boldsymbol{O}_B$, and $\mathbf{R}_z \in \mathrm{SO}(3)$ is the canonical rotation matrix around the axis $\begin{bmatrix}0 & 0 & 1\end{bmatrix}^T$ [29]. The orientation of $\mathcal{F}_{S_i}$ respect to $\mathcal{F}_B$ is given by [25]

$$\mathbf{R}_{S_i}^b(\alpha) = \mathbf{R}_z(\zeta_i)\mathbf{R}_x\Big((-1)^{i-1}\alpha_i(t)\Big) \in \mathrm{SO}(3), \tag{27}$$

where $i = 1, ..., n$, $\alpha_i(t) \in [-\pi/2, \pi/2]$ is the tilt angle of the propellers about $\mathbf{x}_{S_i}$, and $\mathbf{R}_x \in \mathrm{SO}(3)$ is the canonical rotation matrix around the axis $\begin{bmatrix}1 & 0 & 0\end{bmatrix}^T$ [29]. For the case of passively tilting multirotors, $\alpha(t)_i = \alpha_i$ is considered, and it has the same magnitude for each propeller, while $(-1)^{i-1}$ denotes the orientation tilt of each propeller. Figure 2 illustrates the geometric concepts of the length from the propeller to the UAV's CoM and the separation angle between each rotor. Furthermore, the spin direction of each propeller is also displayed, and a front view of the hexarotor is also presented, where the tilting angle α_i about the $\mathbf{x}_{S_i}$ can be appreciated. Each propeller supplies a thrust force applied in $\boldsymbol{O}_{S_i}$ that, expressed in $\mathcal{F}_B$, appears as follow [25]

$$\mathbf{f} = f_i\ \mathbf{R}_{S_i}^b(\alpha)\begin{bmatrix}0 & 0 & 1\end{bmatrix}^T \in \mathbb{R}^3, \tag{28}$$

where $i = 1, ..., 6$, $f_i = k_f \omega_i^2$ is the intensity of the force provided by the i-th angular velocity $\omega_i \in \mathbb{R}$, and $k_f > 0$ is a constant parameter depending on the geometry of the propeller [30]. Simultaneously, the following drag torque is supplied by the propellers [25]

$$\boldsymbol{\tau}_{b_i} = (-1)^{i-1} \sigma \mathbf{f}_{b_i} \mathbf{R}_{S_i}^b(\alpha) \begin{bmatrix} 0 & 0 & 1 \end{bmatrix}^T \in \mathbb{R}^3, \tag{29}$$

where $i = 1, ..., 6$ and $\sigma = k_\tau / k_f$, with $k_\tau > 0$, is a constant parameter depending on the geometry of the propeller and $(-1)^{i-1}$ modelling its spin direction. The total thrust forces applied to the airframe expressed in $\mathcal{F}_W$ are represented by [28]

$$\mathbf{f}_T = \mathbf{R}_b \sum_{i=1}^{6} \mathbf{f}_{b_i} = \mathbf{R}_b \mathbf{F}_1(\boldsymbol{\alpha}) \mathbf{f}, \tag{30}$$

where $\boldsymbol{\alpha} \in \mathbb{R}^n$ contains the titlting angle of each rotor, $\mathbf{f} = \begin{bmatrix} f_1 & \cdots f_n \end{bmatrix}^T \in \mathbb{R}^n$ is the stacking vector of the propeller forces, and $\mathbf{F}_1 \in \mathbb{R}^{3 \times n}$ is a mapping matrix from the propeller forces to the airframe ones. Likewise, the total torques applied to the airframe expressed in $\mathcal{F}_B$ are [30]

$$\boldsymbol{\tau}_T = \sum_{i=n}^{6} \left(\left(\mathbf{p}_{S_i}^b \times \mathbf{f}_{b_i} \right) + \boldsymbol{\tau}_{b_i} \right) = \mathbf{F}_2(\boldsymbol{\alpha}) \mathbf{f}, \tag{31}$$

where $\times$ is the cross product operator and $\mathbf{F}_2 \in \mathbb{R}^{3 \times n}$ is the mapping matrix from the propeller forces to the torques applied to the airframe. Hence, the full allocation matrix is given by

$$\mathbf{F}(\boldsymbol{\alpha}) = k_f \begin{bmatrix} \mathbf{F}_1(\boldsymbol{\alpha}) \\ \mathbf{F}_2(\boldsymbol{\alpha}) \end{bmatrix}. \tag{32}$$

For the case of passively tilted hexarotors it follows that

$$\mathbf{F}_1(\boldsymbol{\alpha}) = \begin{bmatrix} \frac{s_\alpha}{2} & -s_\alpha & \frac{s_\alpha}{2} & -\frac{s_\alpha}{2} & -s_\alpha & -\frac{s_\alpha}{2} \\ \frac{\sqrt{3} s_\alpha}{2} & 0 & -\frac{\sqrt{3} s_\alpha}{2} & \frac{\sqrt{3} s_\alpha}{2} & 0 & -\frac{\sqrt{3} s_\alpha}{2} \\ c_\alpha & c_\alpha & c_\alpha & c_\alpha & c_\alpha & c_\alpha \end{bmatrix},$$

$$\mathbf{F}_2(\boldsymbol{\alpha}) = k_f \begin{bmatrix} \frac{L\sigma_\alpha - \sigma s_\alpha}{2} & \frac{\sqrt{3}(L c_\alpha - \sigma s_\alpha)}{2} & -L s_\alpha - \sigma c_\alpha \\ L c_\alpha - \sigma s_\alpha & 0 & L s_\alpha + \sigma c_\alpha \\ \frac{L c_\alpha - \sigma s_\alpha}{2} & -\frac{\sqrt{3}(L c_\alpha - \sigma s_\alpha)}{2} & -L s_\alpha - \sigma c_\alpha \\ -\frac{L c_\alpha - \sigma s_\alpha}{2} & -\frac{\sqrt{3}(L c_\alpha - \sigma s_\alpha)}{2} & L s_\alpha + \sigma c_\alpha \\ -L c_\alpha + \sigma s_\alpha & 0 & -L s_\alpha - \sigma c_\alpha \\ -\frac{L c_\alpha - \sigma s_\alpha}{2} & \frac{\sqrt{3}(L c_\alpha - \sigma s_\alpha)}{2} & L s_\alpha + \sigma c_\alpha \end{bmatrix}^T.$$

Notice that (32) is static and invertible; therefore, the mapping from the six-dimensional control $\mathbf{u}$ (24) to the actuators forces is

$$\mathbf{f}_b = \mathbf{F}(\boldsymbol{\alpha})^{-1} \mathbf{u}. \tag{33}$$

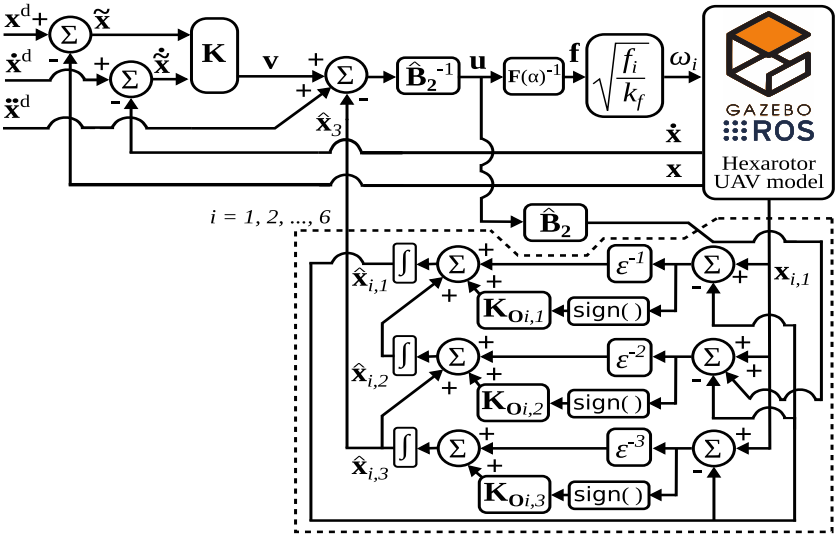

Figure 3. Block diagram of the proposed controller and observer. All within the dashed line is component-wise for $i = 1, 2, ..., 6$.

Finally, the rotor velocities can be computed through

$$\omega_i = \sqrt{\frac{f_i}{k_f}}. \tag{34}$$

4.2. 3D simulation setup

Gazebo dynamic simulator has been used to demonstrate the effectiveness of the proposed approach. In this context, control algorithms have been developed in C++ programming language using Robot Operating System (ROS) as middleware [31]. At the same time, the simulation of the flying platform is based on the library *RotorS* [32]; such a library implements dynamic flying robot models and sensor plugins suitable for Gazebo under ROS and usable for developing custom controllers designed to be analogous to its real-world counterparts so that such simulation is almost transparent with real systems. By default, only flat UAVs are available using *RotorS* software. Therefore, a custom tilted hexacopter has been designed and modelled, taking the well-known *AscTec firefly* platform as inspiration. A significant benefit of the *RotorS* library among the different control and state estimation algorithms is the possibility to simulate UAV rotors with desired motor dynamics and characteristics. In this way, a new multi-copter model can be designed by grouping different rotor models together. Each rotor imported in the simulation scene can be controlled with a desired rotation velocity command, which is consistent with the proposed control approach and allocation. The robot's local position and attitude are available through the ROS network to implement the closed control loop.

The system architecture is depicted in Figure 3, which is discussed in the following. Two main modules have been deployed in the form of ROS nodes: the controller (24) and the observer (25). The latter takes the desired control signal generated by the controller and the multirotor's full pose as input. At the same time, its output is represented by the estimation of the total disturbances acting on the platform. As for the controller, this module receives the platform's pose from the Gazebo simulator and the disturbances estimation provided by the observer to generate the six desired motor control signals expressed in *rpm* (revolutions per minute). In this context, Table 1 reports a list of the controller's parameters and the characteristic of the UAV platform and its motors used to test both the SMC and the ADRC. In particular, $\omega_{i_{max}}$ represents the maximum rotational velocity of the motors, k_f and k_τ represent their drag force and rolling moment constants, respectively, L is the length of the UAV arm, and α is the tilt angle of each rotor. Differently, $\mathbf{K}_{1,...,6}$ and $\mathbf{K}_{7,...,12}$ are the main diagonal components of the feedback gain matrices. It is worth mentioning

that the same proportional and derivative gains were used to test both controllers; the difference is how they reject disturbances, namely, SMC uses the sliding term while ADRC uses the observed signal of the augmented state as feedback. The system has been tested on a standard computer running Ubuntu 20.04 as operating system, while ROS Noetic has been chosen as distribution.

Table 1. List of parameters used for controller implementation and the aerial platform.

Parameter	Value
m	2.1 kg
$\omega_{i_{max}}$	1500 rpm
k_f	8.54858×10^{-6}
k_τ	1×10^{-2}
L	0.215 m
α	20 deg
$\mathbf{K}_{1,\dots,6}$	$\{2, 2, 20, 800, 800, 2500\}$
$\mathbf{K}_{7,\dots,12}$	$\{4, 4, 25, 1200, 1200, 5000\}$

5. Case Studies

This section addresses the tests conducted to assess the effectiveness of the proposed control-observer scheme. First, a complex trajectory is commanded to evaluate the tracking performance; the following experiments consist of a regulation task at a given pose in the presence of external disturbances, which were implemented using a Gazebo external wrench plugin[8]. Finally, a comparison of the proposed controller against a sliding mode controller has been carried out. All the tests are shown in video[9].

5.1. Tracking

This test consists of commanding a complex trajectory to the UAV in Cartesian coordinates with respect to the world frame $\mathcal{F}_W$. The Cartesian position trajectory is given by the following Lemniscate's parametric equations

$$\begin{cases} x_b^d = \dfrac{a\cos(2\pi f_t t)}{1+\sin^2(2\pi f_t t)} \\ y_b^d = \dfrac{a\sin(2\pi f_t t)\cos(2\pi f_t t)}{1+\sin^2(2\pi f_t t)}, \\ z_b^d = bt \end{cases} \tag{35}$$

where $a = 1.4$, $b = 0.2$ are scalar parameters, t is the time, and $f_t = 0.5$ is the frequency in Hz. The time derivatives of (35) were computing numerically. Firstly, the UAV is commanded to take off, thereafter it is commanded to reach $(x_b^d,\ y_b^d,\ z_b^d) = (0, 1.4, 1)$ m with zero orientation, so that it could start and then perform the Lemniscate trajectory, and to end hovering steadily.

Figure 4 shows the norm of the state error $\|\tilde{\mathbf{x}}\|$ during the whole experiment. It can be seen that such a norm is always below 3 cm while the UAV is flying and decreases to zero when it hovers. Furthermore, Figure 5 displays that the UAV trajectory tracks the desired trajectory in the Cartesian space.

5.2. Regulation with Wind and Payload

The robustness of the observer-controller scheme has been assessed by simulating wind conditions while the UAV is hovering at a target set point. The first experiment

[8] https://github.com/Viviana-Morl/ft_gazebo_plugin
[9] https://www.youtube.com/watch?v=TyOvDe81VHc

involves flying the UAV to the set point $(x_b^d,\ y_b^d,\ z_b^d) = (1, 1, 2)$ m with zero orientation and applying an external disturbance some seconds after it reaches the set point. Such a disturbance represents a sudden wind shear given by

$$\mathbf{f}_u = \begin{bmatrix} 0.5 * \text{sign}(\cos(t/2)) \\ 0.5 * \text{sign}(\sin(t/2)) \\ 0 \end{bmatrix} N,\ 38 \leq t \leq 48\ s \tag{36}$$

The top of Figure 6 shows the six controlled states of the UAV during the test. It can be appreciated that the position of the UAV along x_b and y_b axes is affected by the wind shear (36) in a range of ± 15 cm. However, once the wind ends, the states return to the desired values; furthermore, accurate tracking of all the states employing the robust observer is shown. In addition, the bottom of the same figure shows the reconstructed total disturbances affecting the *chain of integrators* that represents the UAV dynamics. The external forces and torques on x_b and y_b can be noticed as well as the effect of the gravity on the UAV. All those signals are obtained using the SMESO (25). Another test, but under soft wind conditions, has been conducted: now, the external disturbances representing a wind blow are given by

$$\mathbf{f}_u = \begin{bmatrix} 0.5\cos(t/2) \\ 0.5\sin(t/2) \\ 0 \end{bmatrix} N,\ 28 \leq t \leq 38\ s. \tag{37}$$

The six controlled and observed states of the UAV's pose are shown at the top of Figure 7. It can be appreciated that the position along x_b and y_b axes is affected ± 5 cm, but returning

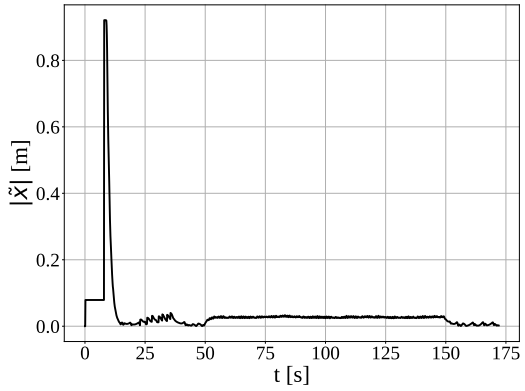

Figure 4. Time evolution of the norm of the state error while the UAV is performing the commanded Cartesian trajectory.

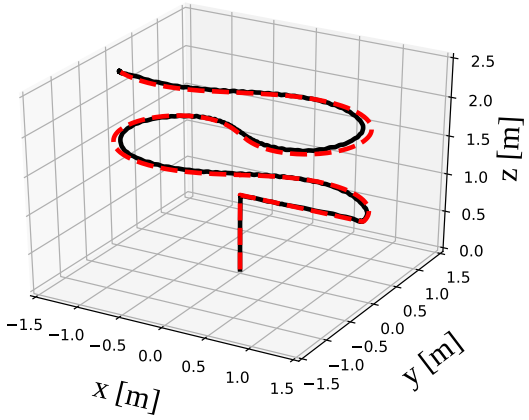

Figure 5. Cartesian motion of the UAV. — — Desired trajectory. – – UAV's trajectory.

to the desired target pose after the wind ends. Alike the Figure 36, the bottom of Figure 7 shows the reconstructed total disturbances using the SMESO (25).

Another experiment was performed to assess the effectiveness of the reconstruction of the disturbances by means of the proposed SMESO. First, the hexarotor is commanded to take-off to 2 m without the node of the SMESO running. Some seconds later the SMESO is turned on and after some time, a -5 N force is applied in the z_B direction for 12 seconds simulating a payload condition. Figure 8 shows the results of the aforementioned

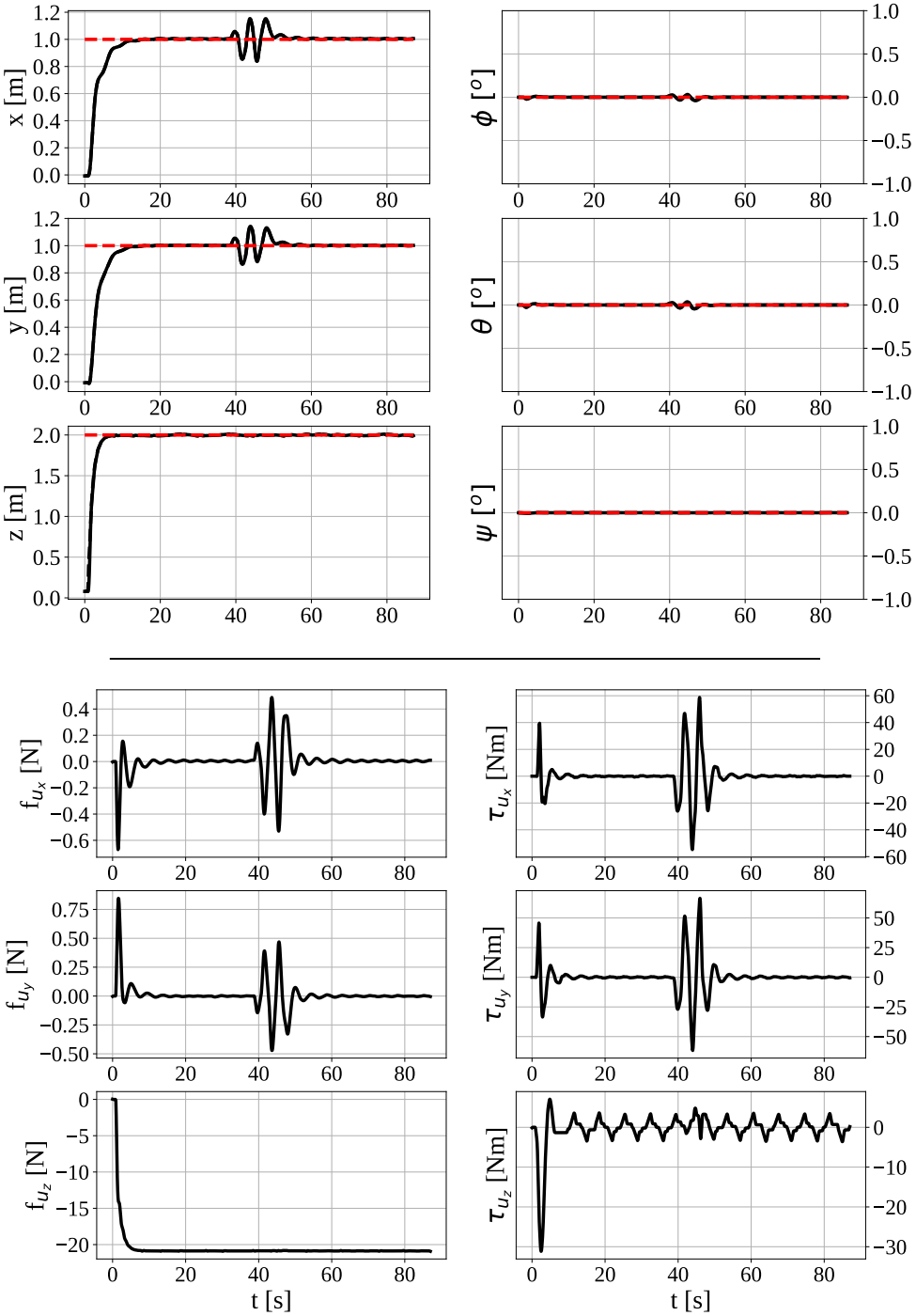

Figure 6. Top: Behaviour of states of the UAV during a regulation task subjected to sudden wind gusts. – – Set points. —- Measured states. — — Observed states. Bottom: Reconstructed total disturbances about each axis.

experiment. The left side of the figure displays the norm of the state error. It can be noticed that, during the take-off without SMESO feedback, the target set point is not achieved and some oscillations are present as well. Afterwards, the norm of the error becomes zero when the SMESO feedback is available. Finally, two peaks of 20 cm can be observed, which occurred when adding and removing the payload force respectively; despite such peaks, the norm of the error was also zero in the meantime the payload was applied. The right side of Figure 8 shows the time evolution of the estimated disturbance along z_B axis. It can be

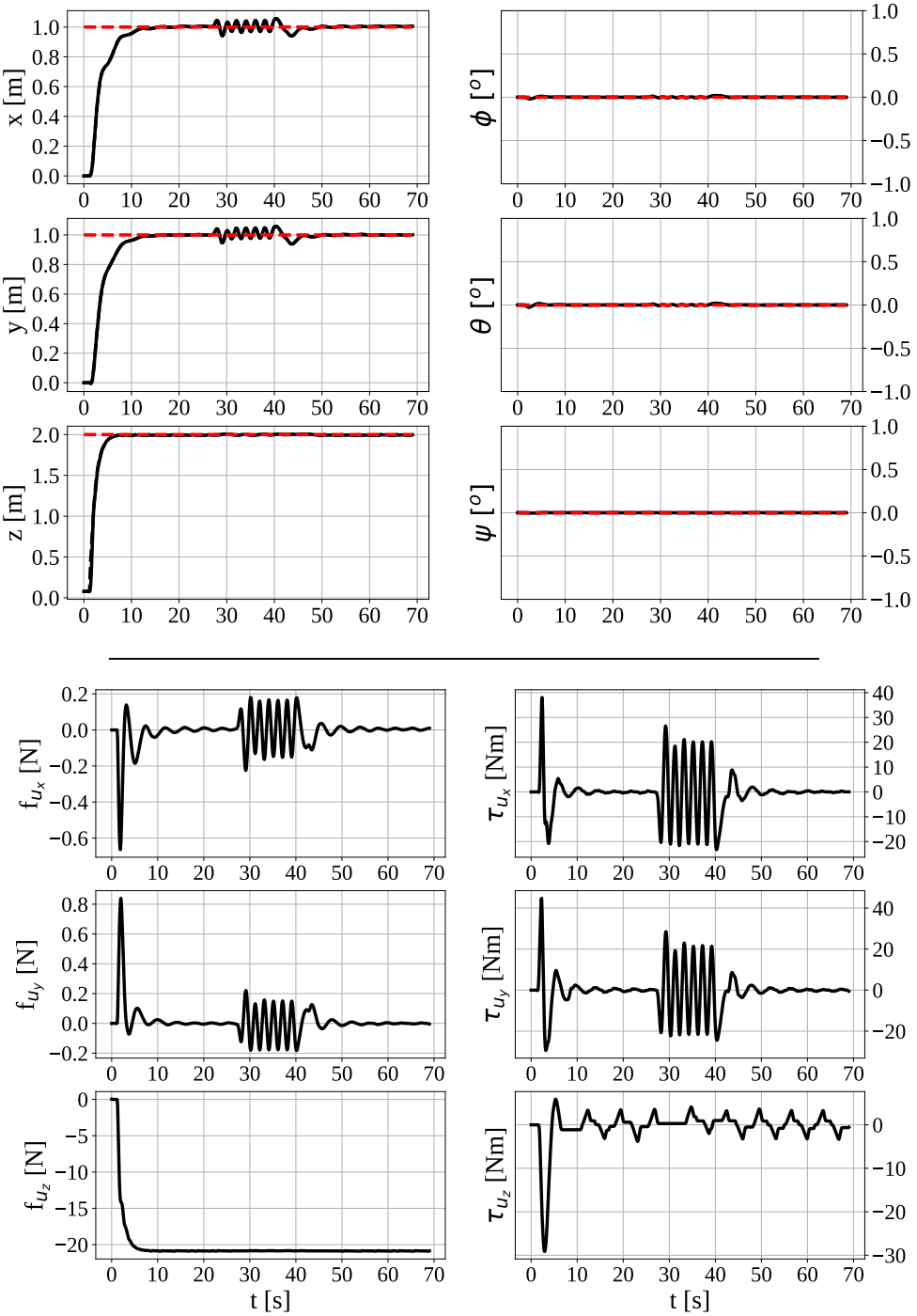

Figure 7. Top: Behaviour of states of the UAV during a regulation task subjected to wind blows. – – Set points. —- Measured states. — — Observed states. Bottom: Reconstructed total disturbances about each axis.

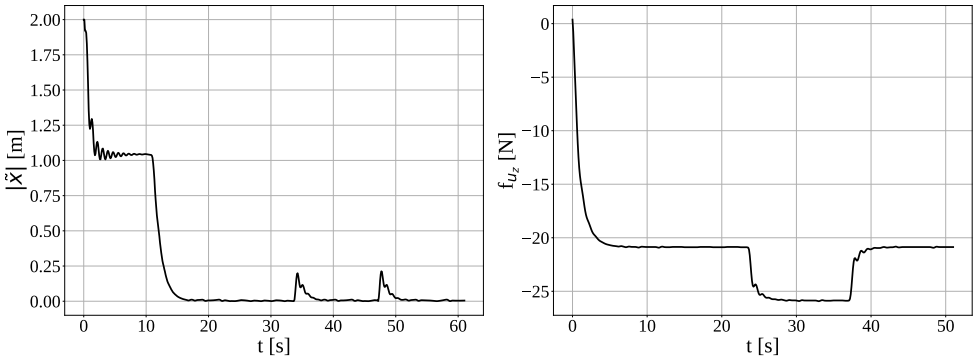

Figure 8. Left: Time evolution of the norms of the state error.
Right: Time evolution of the estimated force along z_B axis, which is retrieved from the SMESO.

appreciated that the SMESO supplies a signal of -20,6 N, which is consistent with the total weight of the hexarotor, since the controller (24) does not include gravity compensation. In addition, it can be noticed that the SMESO provided a signal of -25,6 N while the payload was being applied, thus, the external disturbances were effectively reconstructed with the proposed SMESO.

5.3. Comparison Against Sliding Mode Control

Finally, the proposed controller performance has been compared against the SMC given by

$$\mathbf{u} = \mathbf{B}_2^{-1}\mathbf{K}\left[\text{sign}(\mathbf{s})^T \ -\dot{\mathbf{x}}^T\right]^T, \tag{38}$$

where $\mathbf{K}$ has the same values as in Table 1, and the $\mathbf{s} = \text{diag}(2,2,10,20,20,20)\tilde{\mathbf{x}} - \dot{\mathbf{x}}$ is the sliding surface. The UAV is commanded to the target set point $(x_b^d,\ y_b^d,\ z_b^d) = (0,0,2)$ m with 10 deg of orientation about z_b for 20 seconds.

Figure 9 shows the norms of the error using both controllers. Even though both controllers provide a stable behaviour of the norm of the error, a steady-state error of 5 cm can be appreciated with SMC.

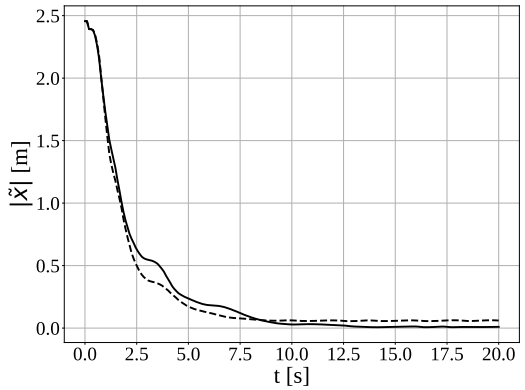

Figure 9. Time evolution of the norms of the state error while the UAV is performing a regulation task. —- ADRC. − − SMC.

6. Conclusion

A robust control scheme for full pose regulation and tracking of a passively tilted hexarotor UAV was presented in this work. The main contribution is implementing a theoretical-sustained ADRC approach with a robust SMESO on a passively tilted hexarotor employing a highly realistic simulator. It is worth highlighting that such a technique has not been reported in the literature for passively tilted hexarotors. Furthermore, the stability analysis of both the designed controller and observer was presented using a consistent

theory that does not rely on *a priori* knowledge of the total disturbance bound as several ADRC schemes do in the literature. As mentioned above, a simulator with physics motors was used during the presented work, which behaviour is almost identical to the real UAV. In order to prove the effectiveness of the control system proposal, several case studies were carried out. Achieving the target trajectory was successful since all the states reached the target value with errors close to zero. Additionally, the proposed controller was effective upon payload and continuous time-varying and discontinuous wind disturbances simulation thanks to the perfect reconstruction of the external disturbances, which is consistent with the theoretical hypothesis of the convergence of the observer regarding the non-differentiable total disturbance. The proposed controller yielded a recovery time fewer than five seconds, achieved the set point with a significantly low overshoot for the worst case, and remained within an acceptable range upon solid disturbances. The presented control approach performed better than the SMC because it yielded significantly less steady-state norm of the error for full pose regulation. These successful results prove the effectiveness of the proposed control technique and motivate its application to other UAVs.

Author Contributions: Conceptualisation, S.O.; methodology, S.O.; software, S.O. and J.C.; validation, S.O.; formal analysis, S.O. and F.R.; investigation, S.O.; resources, V.L.; data curation, S.O.; writing—original draft preparation, S.O; writing—review and editing, S.O., J.C., F.R. and V.L.; visualisation, S.O.; supervision, F.R. and V.L.; project administration, V.L.; funding acquisition, F.R. and V.L.. All authors have read and agreed to the published version of the manuscript.

Funding: The research leading to these results has been supported by the AERIAL-CORE project (Horizon 2020 Grant Agreement No. 871479). The authors are solely responsible for its content.

Institutional Review Board Statement: Not applicable.

Informed Consent Statement: Not applicable.

Data Availability Statement: Not applicable.

Conflicts of Interest: The authors declare no conflict of interest.

References

1. Lee, S.J.; Kim, S.; Johansson, K.H.; Kim, H.J. Robust acceleration control of a hexarotor UAV with a disturbance observer. In Proceedings of the 2016 IEEE 55th Conference on Decision and Control (CDC). IEEE, 2016, pp. 4166–4171.
2. Dai, B.; He, Y.; Zhang, G.; Gu, F.; Yang, L.; Xu, W. Wind disturbance rejection for unmanned aerial vehicle based on acceleration feedback method. In Proceedings of the 2018 IEEE Conference on Decision and Control (CDC). IEEE, 2018, pp. 4680–4686.
3. Li, D.; Liu, H.H. Sensor bias fault detection and isolation in a large multirotor aerial vehicle using active disturbance rejection control. In *2018 AIAA Information Systems-AIAA Infotech@ Aerospace*; AIAA, 2018; p. 0249.
4. Ding, L.; Zhou, J.; Shan, W. A hybrid high-performance trajectory tracking controller for unmanned hexrotor with disturbance rejection. *Transactions of the Canadian Society for Mechanical Engineering* **2018**, *42*, 239–251.
5. Arellano-Quintana, V.M.; Portilla-Flores, E.A.; Merchán-Cruz, E.A. Multi-objective design optimization of a hexa-rotor with disturbance rejection capability using an evolutionary algorithm. *IEEE Access* **2018**, *6*, 69064–69074.
6. Chen, Z.; Stol, K.; Richards, P. Preliminary design of multirotor UAVs with tilted-rotors for improved disturbance rejection capability. *Aerospace Science and Technology* **2019**, *92*, 635–643.
7. Xu, H.; Yang, Z.; Lu, K.; Xu, C.; Zhang, Q. Control of a Tilting Hexacopter under Wind Disturbance. *Mathematical Problems in Engineering* **2020**, *2020*.
8. Kotarski, D.; Piljek, P.; Brezak, H.; Kasać, J. Chattering-free tracking control of a fully actuated multirotor with passively tilted rotors. *Transactions of FAMENA* **2018**, *42*, 1–14.
9. Yao, C.; Krieglstein, J.; Janschek, K. Modeling and Sliding Mode Control of a Fully-actuated Multirotor with Tilted Propellers. *IFAC-PapersOnLine* **2018**, *51*, 115–120.
10. Arizaga, J.M.; Castañeda, H.; Castillo, P. Adaptive Control for a Tilted-Motors Hexacopter UAS Flying on a Perturbed Environment. In Proceedings of the 2019 International Conference on Unmanned Aircraft Systems (ICUAS). IEEE, 2019, pp. 171–177.
11. Nguyen, N.P.; Kim, W.; Moon, J. Super-twisting observer-based sliding mode control with fuzzy variable gains and its applications to fully-actuated hexarotors. *Journal of the Franklin Institute* **2019**, *356*, 4270–4303.
12. Kase, S.; Oya, M. Adaptive tracking controller for hexacopters with a wind disturbance. *Artificial Life and Robotics* **2020**, pp. 1–6.

13. Rashad, R.; Kuipers, P.; Engelen, J.; Stramigioli, S. Design, modeling, and geometric control on SE (3) of a fully-actuated hexarotor for aerial interaction. *arXiv preprint arXiv:1709.05398* **2017**.
14. Rashad, R.; Califano, F.; Stramigioli, S. Port-Hamiltonian passivity-based control on SE (3) of a fully actuated UAV for aerial physical interaction near-hovering. *IEEE Robotics and automation letters* **2019**, *4*, 4378–4385.
15. Ryll, M.; Muscio, G.; Pierri, F.; Cataldi, E.; Antonelli, G.; Caccavale, F.; Bicego, D.; Franchi, A. 6D interaction control with aerial robots: The flying end-effector paradigm. *The International Journal of Robotics Research* **2019**, *38*, 1045–1062.
16. Huang, Y.; Xue, W. Active disturbance rejection control: methodology and theoretical analysis. *ISA transactions* **2014**, *53*, 963–976.
17. Guo, B.Z.; Zhao, Z.L. On convergence of non-linear extended state observer for multi-input multi-output systems with uncertainty. *IET Control Theory & Applications* **2012**, *6*, 2375–2386.
18. Sira-Ramírez, H.; Luviano-Juárez, A.; Ramírez-Neria, M.; Zurita-Bustamante, E.W. *Active disturbance rejection control of dynamic systems: a flatness based approach*; Butterworth-Heinemann, 2018.
19. Guo, B.Z.; Zhao, Z.L. *Active disturbance rejection control for nonlinear systems: An introduction*; John Wiley & Sons, 2016.
20. Orozco-Soto, S.M.; Ibarra-Zannatha, J.M. Motion control of humanoid robots using sliding mode observer-based active disturbance rejection control. In Proceedings of the 2017 IEEE 3rd Colombian Conference on Automatic Control (CCAC). IEEE, 2017, pp. 1–8.
21. Spurgeon, S.K. Sliding mode observers: a survey. *International Journal of Systems Science* **2008**, *39*, 751–764.
22. Drakunov, S.; Utkin, V. Sliding mode observers. Tutorial. In Proceedings of the Proceedings of 1995 34th IEEE Conference on Decision and Control. IEEE, 1995, Vol. 4, pp. 3376–3378.
23. Patel, R.V.; Toda, M.; Sridhar, B. Robustness of linear quadratic state feedback designs in the presence of system uncertainty. *IEEE Transactions on Automatic Control* **1977**, *22*, 945–949.
24. Khalil, H.K. *Nonlinear systems*; Prentice Hall, 2002.
25. Michieletto, G.; Ryll, M.; Franchi, A. Fundamental actuation properties of multirotors: Force–moment decoupling and fail–safe robustness. *IEEE Transactions on Robotics* **2018**, *34*, 702–715.
26. Ruggiero, F.; Cacace, J.; Sadeghian, H.; Lippiello, V. Passivity-based control of VToL UAVs with a momentum-based estimator of external wrench and unmodeled dynamics. *Robotics and Autonomous Systems* **2015**, *72*, 139–151.
27. Poznyak, A.; Polyakov, A.; Azhmyakov, V. *Attractive ellipsoids in robust control*; Springer, 2014.
28. Ryll, M.; Bicego, D.; Franchi, A. Modeling and control of FAST-Hex: A fully-actuated by synchronized-tilting hexarotor. In Proceedings of the 2016 IEEE/RSJ International Conference on Intelligent Robots and Systems (IROS). IEEE, 2016, pp. 1689–1694.
29. Siciliano, B.; Sciavicco, L.; Villani, L.; Oriolo, G. *Robotics: modelling, planning and control*; Springer Science & Business Media, 2010.
30. Rajappa, S.; Ryll, M.; Bülthoff, H.H.; Franchi, A. Modeling, control and design optimization for a fully-actuated hexarotor aerial vehicle with tilted propellers. In Proceedings of the 2015 IEEE international conference on robotics and automation (ICRA). IEEE, 2015, pp. 4006–4013.
31. Joseph, L.; Cacace, J. *Mastering ROS for Robotics Programming - Second Edition: Design, Build, and Simulate Complex Robots Using the Robot Operating System*, 2nd ed.; Packt Publishing, 2018.
32. Furrer, F.; Burri, M.; Achtelik, M.; Siegwart, R., RotorS - A Modular Gazebo MAV Simulator Framework; Springer Verlag, 2016; Vol. 625, chapter Robot Operating System (ROS), pp. 595–625. https://doi.org/10.1007/978-3-319-26054-9_23.